CARBON NANOTUBE STRAIN SENSORS WITH WIDE DYNAMIC RANGE FABRICATED ON FLEXIBLE SUBSTRATES BY NOVEL PROCESSING TECHNIQUES

BY

HYUNJONG JIN

THESIS

Submitted in partial fulfillment of the requirements
for the degree of Master of Science in Electrical and Computer Engineering
in the Graduate College of the
University of Illinois at Urbana-Champaign, 2009

Urbana, Illinois

Adviser:

Professor Kanti Jain

ABSTRACT

Carbon nanotube (CNT) strain sensors on flexible polyimide substrates with novel fabrication techniques have been fabricated. Excimer laser photoablation was used for simultaneous patterning of the CNT layer and the polyimide substrate. A transferring technique utilizing sacrificial etching was used for clear material transfer. Clear patterns free of CNT-polymer composites were made and were successfully transferred to a flexible substrate. The resulting device has a gauge factor of 60, which is comparable to the 50~150 value for silicon strain sensors. The device exhibits a dynamic range of up to 1.5% strain, far superior to the 0.03% of silicon.

ACKNOWLEDGMENTS

I would like to begin by thanking my adviser, Professor Kanti Jain, for his support and guidance in carrying out my graduate research. I would like to thank him profusely for giving me an opportunity to work with him.

I would like to extend my sincere thanks to Dr. Junghun Chae and Mr. Kevin Lin for working with me on the experiment of excimer laser ablation.

I would like to thank my mother, Mrs. Hee Sook Kwun-Jin, for her insight and encouragement which have been the pillars of strength throughout my life. I would like to thank my father, Dr. Min Jin, for his unconditional support and guidance which have enabled me to become who I am this day.

TABLE OF CONTENTS

LIST OF FIGURES

Figure Page

CHAPTER 1

INTRODUCTION

Sensors transform various stimulus signals in various energy domains (such as thermal, mechanical, chemical, radiative, or magnetic) to the electrical domain. The capability of transforming those signals into the electrical domain enables perception and processing via electronic devices. Large-area multimodal sensor arrays have been pursued to increase the density of sensor nodes and enhance the measurement resolution. The massive amounts of data gained by sensor arrays provide multimodal information about the environment, such as temperature, pressure, humidity, strain, and chemical composition. These sensor arrays have applications such as structural health monitoring (SHM) of vehicles and infrastructure [1-7], tactile feedback for robotics [8-9], electronic textiles for patient, soldier, and athlete health monitoring [10-13], and low-cost sensors for consumer applications [14-16].

Among these sensor applications, there is a growing interest in SHM of various infrastructures. The importance of managing aging infrastructures has gained the public's interest, in light of catastrophic incidents such as the I-35W Mississippi River bridge collapse in Minneapolis, MN, in 2007. The need to include automated damage detection capability within the design of an infrastructure leads to the concept of SHM. This issue also becomes more important as new structures are increasingly made of composite materials. Unlike metal structures, composites are more prone to internal damage while showing no visible surface

damage, thereby rendering visual inspection ineffective [1]. The inherent localized nature of structural damage is another important factor. Because damage from cracks and plastic deformation occurs at localized positions, locally based monitor approaches will enhance the accuracy of SHM.

Currently, SHM is performed manually using ultrasonic and other physical detection techniques, which are time-consuming and expensive. This cost barrier has limited the total number of sensors installed. However, development of low cost sensors and the use of wireless sensors encourage the deployment of more sensors in a single SHM system, thus increasing the resolution of the system. One of the most promising ways to achieve effective health monitoring of structures is the development of large-area strain sensor skins that can be integrated into the surface and act as a highly responsive, complex nervous system. Such a system would provide a cost-effective monitoring capability that is more thorough and reliable than current techniques. One of the impediments in implementation of electronic sensor arrays for SHM is the lack of large-area manufacturing and integration capabilities that would utilize the enormous potential of such systems. Also, the installation of conventional strain sensors on curved surfaces has had limited success because conventional sensor arrays have limited conformability. To increase the viability and practicality of large-area sensor arrays, they must be flexible, robust, and conformable to many surfaces. To be practical and commercially viable, these sensor arrays must be fabricated on a large-area scale at a low cost. MEMS technology has traditionally utilized bulk micromachining and surface micromachining of silicon to produce sensors and actuators [17], so the technology for flexible substrates and flexible sensor arrays is still in its infancy. For this, metal gauges have been widely used to measure component strains, both in research and in the industry.

The most common and conventional strain sensor is the metal strain gauge. A metal strain gauge consists of a thin film of metal on a polymer substrate. The strain from the environment will change the width and length of the gauge, thus inducing an electrical resistance change. While such devices serve as low cost sensors for SHM, they suffer from performance limitations. For example, the low gauge factors limit the measurement resolution, making the accurate measurement of low level strain difficult. Furthermore, the typical dynamic range of less than 0.4% [17] limits the operation range of the device. Lastly, problems with temperature sensitivity and long-term stability of metal gauges make this approach non-ideal for deployment of sensors in locations that are difficult for frequent manual maintenance. Hence, for effective SHM, single-walled carbon nanotube (SWCNT) strain sensors with superior mechanical properties have gained the interest of the research community.

The goal of this research is to develop a large-area, flexible, highly stretchable sensor array that can be integrated into unconventional surfaces with minimum modifications to existing systems, so that strain sensor arrays can be integrated into both new and existing structures. A flexible polymer material has been used as a low-cost, large-area substrate. A new transfer technique provides both ease of fabrication and mechanical functionality compared to previously seen stamping methods [18-20]. Carbon nanotubes (CNTs) are used as the strain sensing material to provide high sensitivity and maximum flexibility. The conformability of the sensor arrays will also be maximized, allowing the sensor arrays to be installed on sharply curved surfaces.

CHAPTER 2

BACKGROUND

In this section, current technologies that are used in the development of strain sensors are reviewed. Conventional strain gauges for SHM are introduced. An overview of the characteristics of carbon nanotubes (CNTs) is presented. Attributes of CNT strain sensors from the functional background to recent demonstrations of the concept are discussed. Finally, the conventional fabrication processes and technologies for CNT devices are presented, and their disadvantages are discussed.

2.1 Current Strain Sensor Technologies

Structural health monitoring (SHM) systems have been suggested not only for infrastructures such as bridges, buildings, and pipelines, but also for aircraft and spacecraft. The wide application range results in deployment of these sensors in diverse environments. Thus, the characteristics of present strain sensor technologies must be addressed in order to provide solutions for the technological difficulties SHM faces. Understanding this will be the prerequisite for presenting these new opportunities with novel technologies.

2.1.1 Electrostatic sensors

At the heart of electrostatic sensors are capacitors, broadly defined as two conducting surfaces that can hold charges of opposite polarity. The most common geometry is parallel plate, in which two parallel metallic plates sandwich a dielectric. With this geometry mounted vertically on a sensing target substrate, electrostatic sensors can detect changes in capacitance caused by the variation in the relative position of the two conductors. The readout circuitry translates that change into electrical signals, enabling the sensing of strain and physical displacement.

The sensitivities of these sensors are proportional to the overlapping area of the parallel surfaces. Hence, a common method to improve the electrostatic sensor is to increase the coupling area of the surfaces. These enhanced devices involve the use of interdigitated finger (IDT) capacitors [17]. Two comb-like features overlap each other with a slight displacement so that a finger from one side partially fills the void of the other. Because the two combs have opposite charges, adjacent fingers have opposite polarities. This results in multiple conducting surfaces performing as a single capacitor, increasing the effective coupling area and the sensed capacitance.

The sensitivity of the electrostatic sensor is inversely proportional to the distance between the plates. Therefore, for tracking strain levels of ~0.1%, micro-scale or nano-scale devices will provide higher sensitivity since the change of capacitance will be relatively greater.

While the electrostatic approach provides great simplicity, low operating power, and fast response, there is an inherent difficulty in monitoring long term displacements. Sensitivity to vibration also makes electrostatic strain sensors impractical for SHM applications [17].

2.1.2 Piezoresistive sensors

The piezoresistive effect refers to the change in resistance upon an induced strain and deformation. This sensor type utilizes two types of mechanisms: the change in the dimension (such as length and cross section) of the conductive path itself and the change in the bulk resistivity of the piezoresistive material. Depending on the sensor design and material, one effect may be dominant over the other. By strict definition, *piezoresistors* refer to devices in which change in resistance is caused by alteration in resistivity. In these materials, the magnitude of resistance change is much greater than that from the change in dimension [17]. A device in which resistance change is mainly by the dimension deformation is referred to as a strain gauge (Fig. 2.1). From a broad point of view, both sensors may be categorized as piezoresistive sensors.

Conventional materials that are utilized for piezoresistive sensors are metals, crystalline silicon, and polysilicon. In the case of a metal strain sensor, the sensing mechanism is based on differences in the conductive dimensions. Upon mechanical strain and elongation, the conductive path length increases and the cross-sectional area decreases, thus increasing the resistivity of the device. For single-crystal or polycrystalline silicon, stretching the conductive trace will change its conductivity drastically. These sensors can be used for inertia sensors, pressure sensors, flow sensors, and tactile sensors [21, 22].

2.1.3 Piezoelectric sensors

Piezoelectric materials generate an electric charge or voltage when subjected to mechanical stress. These materials also produce mechanical deformation when an external electric field is applied. The important properties of these materials come from their microcrystalline structures. Piezoelectric crystals may be observed as a collection of separate

crystalline domains. The polarization direction of each domain is randomly distributed; hence, no overall polarization is specified. When a crystal is exposed to a strong electric field at an elevated temperature, a process called poling, domains within the crystal most nearly aligned with the field will grow and dominate the other crystal domains. This results in a net polarization of the material. When the electric field is removed, the dipoles remain locked in an approximate alignment, giving the crystal a remnant polarization. Materials showing such characteristics include quartz, AlN (aluminium nitride), ZnO (zinc oxide), and PZT (lead zirconate titanate). Applications of the piezoelectric sensor include inertia sensor, acoustic sensor, tactile sensor, flow sensor, surface elastic wave sensor, and energy harvesting [17].

Depolarization occurs if the piezoelectric material is subjected to a strong opposing electric field. Depolarization also occurs when the orientation of the crystal domains is altered significantly, by either mechanical stress or thermal effects. The change in the crystal domain orientation may destroy the dipole alignments, causing the material to depolarize. Sensors for SHM applications are expected to have long maintenance intervals and high reliability; thus, the depolarization of the piezoelectric material causes stability concerns.

2.1.4 Optical sensors

Optical sensors use the deformation of fiber optic wires embedded in infrastructure to detect any abnormalities in the structure. Some of the common methods of optical sensing include analysis by Fabry-Perot cavities, use of fiber Bragg gratings (FBGs), and Brillouin scattering [23]. Fabry-Perot cavity sensors have a small gap (a few microns) between the ends of two fibers that are partially reflective, so the transmitted and reflected spectrum of light is a function of the gap distance. Therefore, physical dislocations in the range of fractions of

wavelengths can be accurately measured by determining the size of the gap between the fibers. Fiber Bragg gratings have periodic changes in the index of refraction of the fiber that act as a filter such that one frequency is reflected while other frequencies are transmitted. The reflected frequency of the fiber is a function of the strain in the fiber, and therefore changes with the periodicity of the fiber. Brillouin scattering fiber optic sensors rely on characterizing the reflected spectra of fiber optic wires to determine the presence and location of structural failures; damaged fibers show a broader reflected spectrum and thus indicate failure [24, 25]. Although it is an attractive sensing strain method, the relative complexity and the narrow dynamic range hinder the application of optical strain sensors for SHM.

2.2 Carbon Nanotubes for Strain Sensing

Many materials with piezoelectric, piezoresistive, or other sensing properties can be used as strain gauges. However, these conventional materials have various limitations on their use in conformal environments; these limitations include the need for high excitation voltages, material brittleness, and a small dynamic range that reduces sensor effectiveness. Carbon nanotubes (CNT) are one of the candidates for overcoming these limitations. CNTs have excellent mechanical, electrochemical, and piezoresistive properties that make them strong candidates for strain sensing applications for SHM [26].

2.2.1 Basic properties of CNTs

CNTs are cylindrical nanostructures made of carbon. They can be conceptualized as rolled up sheets of graphene, one-atom-thick layers of carbon. Carbon atoms are placed in a

repeating hexagonal pattern, with one carbon atom at each edge. The chemical bonding is composed of sp^2 bonds, which provide the basis for the unique mechanical strength of CNTs [27]. The typical CNT diameter is approximately 1 nm for a single-walled CNT (SWCNT). In terms of electrical characteristics, CNTs may be either metallic or semiconducting, depending on the chirality of the structure. In practice, approximately one third of the CNTs are metallic; the remaining two thirds are semiconducting. Generally, both metallic and semiconducting CNTs are synthesized together. This means that synthesized CNT samples will have randomly distributed metallic and semiconducting CNTs mixed together.

Carbon nanotubes have an even higher tensile strength than that of high-carbon steel. The high electrical conductivity (1000 times greater than that of copper), thermal conductivity (100 times higher than that of diamond) and mechanical strength enable CNTs to exceed the performance of many conventional engineering materials. However, since the cross-sectional area of a CNT is in the nanoscale, the electrical and thermal conductance of an individual CNT is not as high as those of other materials [27].

2.2.2 Piezoresistive behavior of individual CNT

The piezoresistive behavior of the CNT strain sensor originates from defects in the CNT structure. Theoretically, CNTs are made with a continuous hexagonal structure; however, topological defects like pentagons and octagons are present in actual CNTs. Under applied stress, a nanotube is deformed, and the dislocations result in different electrical properties exhibited by the CNT. There is an associated change in the band gap, which is inversely proportional to the diameter of the CNT. Therefore, when strain and agitation energy are applied, dislocations and defects occur within the CNT, changing the conductivity [28].

2.2.3 Carbon nanotube nanonet

It is not practical to use individual CNT tubes as the sensing material for strain sensors. Individual CNTs are difficult to align on a large scale and have limited maximum length. Also, the fracture of a single CNT tube due to mechanical fatigue or any other reason will result in the failure of the device itself. Another shortcoming of using individual nanotubes is the variation from one tube to the next: their slightly different forms result in different performance characteristics.

To overcome these limitations, many tubes may be used together. A two-dimensional random network of multiple nanotubes forms a CNT nanonet (Fig. 2.2). This does not require alignment of individual nanotubes, easing the fabrication process. Also, the CNT nanonet is tolerant to mechanical fatigue because there will be multiple conductive pathways such that the device remains electrically conductive even if one pathway is damaged. The use of multiple nanotubes averages the differences between individual tubes, such that any shortcoming in one of the tubes may be compensated by a better performing tube.

The introduction of nanonet for CNT strain sensor introduces another piezoresistive sensing mechanism. The resistance of the CNT strain sensor is affected not only by dislocations within a single nanotube, but also by the relative positioning of adjacent CNTs, which determines the effective electrical characteristics of the conducting path. This allows a wider dynamic range of strain measurement. The buckypaper and CNT-polymer composite both utilize this concept of the CNT nanonet [29, 30].

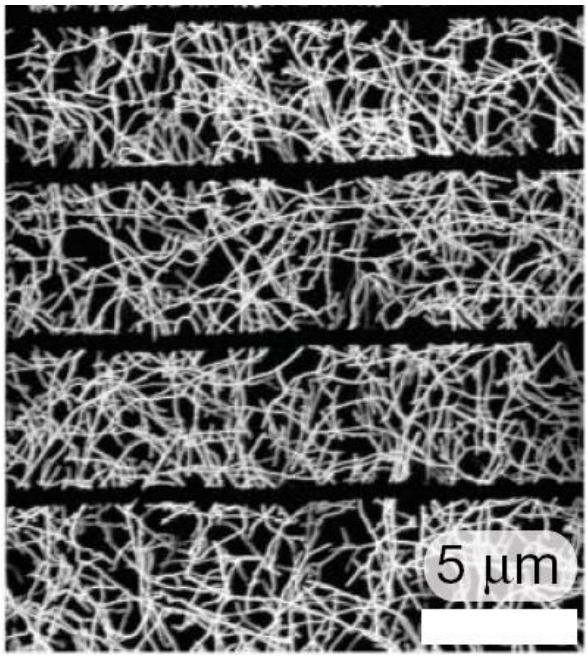

Figure 2.1 Carbon nanotube nanonet [20].

2.3 Fabrication Approach for Conventional CNT Devices

The fabrication process for CNT devices on flexible substrate involves synthesis, patterning, and transferring of devices. Synthesis is done by utilizing a catalyst in a high temperature, carbon rich environment. Since a temperature as high as 1000 ^{o}C is required for CNT synthesis, direct growth on a flexible substrate is not possible. There are several previous approaches that address this fabrication difficulty.

2.3.1 Synthesis of carbon nanotubes

Since the first observation of CNTs in 1991, there has been extensive research towards controlled growth of CNTs. Technologies such as arc discharge, laser ablation, and chemical vapor deposition (CVD) have been developed. In arc discharge, high currents are passed through

opposing carbon anodes and cathodes. For SWCNT growth, a small percentage of metal catalyst is incorporated within the cathode material. The laser ablation method uses intense laser pulses to ablate a carbon target with metal catalysts. This effectively heats the sample up to 1200 ^{o}C. An inert gas is introduced to decrease the contamination. While these approaches result in CNT synthesis of large quantities, a purification process is required [26].

The chemical vapor deposition (CVD) approach uses a substrate prepared with a metal catalyst of a few angstroms thickness, most commonly Ni, Co, or Fe. The substrate is introduced into the CVD chamber. As the temperature of the CVD chamber increases, the catalyst melts to form many sets of spherical balls. When a hydrocarbon gas is introduced into the chamber, CNTs form at the catalyst balls. The density may be controlled by the type of gas introduced, the temperature of growth, and also the time. This approach provides a higher degree of freedom in patterning, due to the capability of patterning the catalyst layer prior to growth [26].

2.3.2 Concept of the CNT-polymer composite and buckypaper approach

One method to realize the CNT nanonet concept is to form a CNT-polymer composite, in which the CNTs may be incorporated within a polymer matrix composite either by shear mixing with an epoxy or by spinning on a polymer layer and a CNT layer subsequently. The CNT-polymer composite method improves the interfacial adhesion between the substrate and the sensing CNT layer. This increases the strain transfer, enabling a more accurate sensor [31].

Another method to form a nanonet of CNTs is the buckypaper CNT (Fig. 2.3). Buckypaper CNTs are formed when a solution such as dimethyl formamide (DMF) is poured into a filter paper, or a Teflon casting mold, and dried in vacuum. This produces a buckypaper with incorporated carbon nanotubes which can be handled easily. However, buckypaper CNT

strain sensors are subjected to slipping upon strain. This may dampen the strain transfer from the domain of interest to the buckypaper sensor region. Thus, the limitation in transferring strain to the nanotubes in the buckypaper makes it disadvantageous for strain sensing application [31].

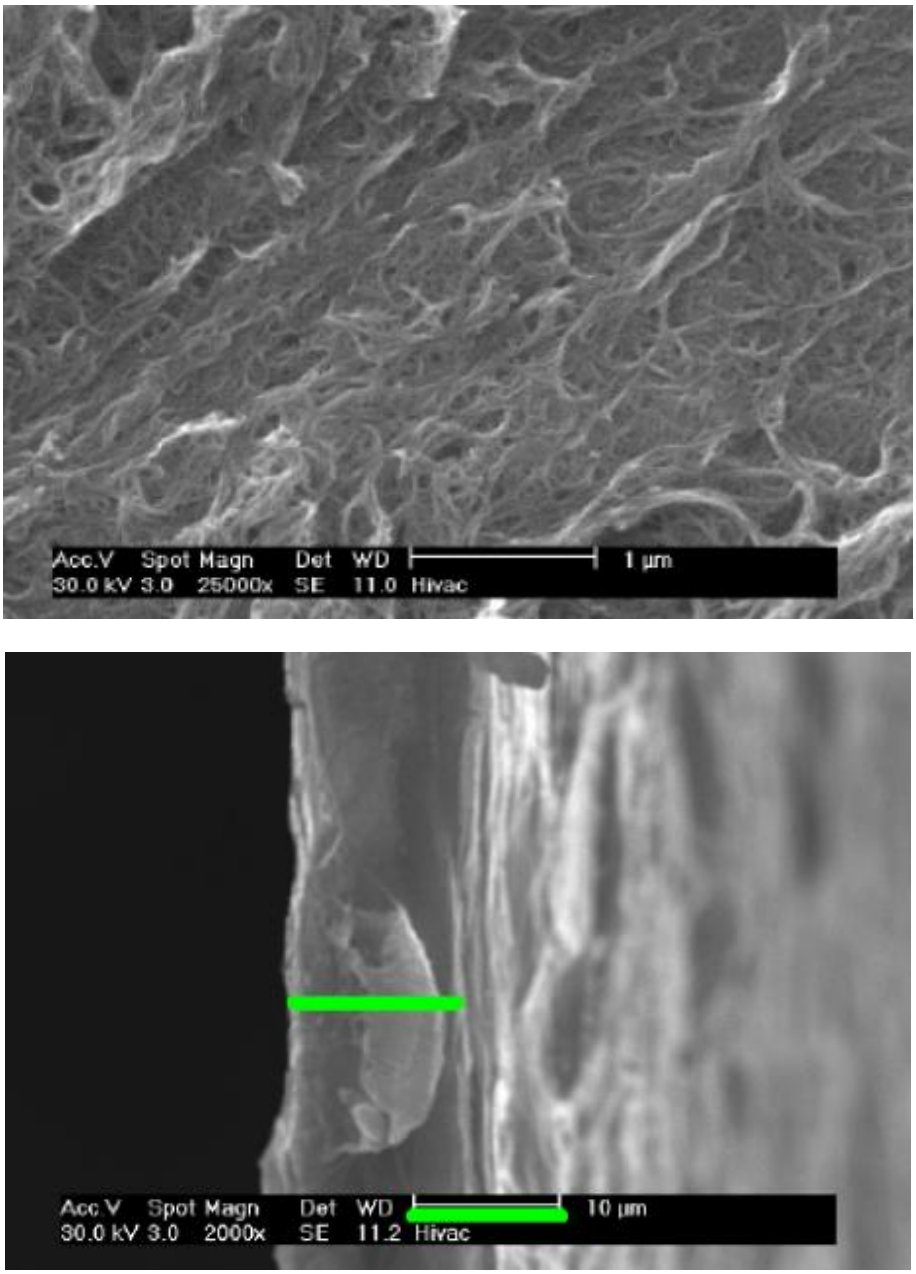

Figure 2.2 Buckypaper approach [31].

2.3.3 Device transferring on flexible substrates

Transferring has been a prominent research area that enables use of high temperature fabrication steps for flexible electronics. Devices are first fabricated by conventional technologies on a donor substrate. The device features are then transferred to a target substrate. Stamping, a transferring method, has been previously demonstrated with silicon ribbons, SWCNTs, GaN nanowires and GaAs nanowires [18, 19]. Device features are first transferred to a stamp, which is then used again to transfer the features to the target flexible substrate. The process is well illustrated for silicon ribbon fabrication. Silicon structures can be mounted on pre-stretched elastomers, forming ribbons and other flexible structures after the release of these elastomers [13, 18, 19]. These structures are then transferred from the elastomer stamp to the target flexible substrate. The primary force that drives stamping is the difference between the adhesion of the substrate and device features. Features are transferred by increasing adhesion to the target substrate and decreasing adhesion to the donor. This stamping method requires three substrates (donor, stamp, and final target flexible substrate) and it requires a minimum of two transferring steps. This fabrication complexity increases the probability of error because of the difference in adhesion and also the requirement of two steps. In other transfer methods, wet etch release of sacrificial layers is utilized in transferring device features [19]. Although this method is more stable, it limits the size of the substrate because large-area substrates require more time to etch the entire sacrificial layer and release the substrate.

2.3.4 Limitations of previous approaches

Buckypaper CNT strain sensors have the problem of non-efficient strain transfer due to slipping of individual tubes. Polymer-CNT composites have been demonstrated on flexible

substrates to improve strain sensitivity, but have not been tested for maximum conformability. The final product must be not only stretchable, but also bendable at sharp angles for maximum conformability. Also, the use of solution-based CNTs, as in the case of forming buckypaper, has the disadvantage of being exposed to excessive vibrational energy. Powder CNTs must be dispersed in a solution using the mechanical dispersion of ultrasonic or shear force mixing. This process may fragment the nanotubes, reduce the aspect ratio and degrade the electrical properties of the nanotubes [30, 31, 32].

CHAPTER 3

DESIGN AND FABRICATION OF CARBON NANOTUBE STRAIN SENSORS ON FLEXIBLE SUBSTRATES

To address the limitations of previous strain sensors and carbon nanotube (CNT) based sensors, we explore the capabilities of the CNT strain sensors fabricated by a novel patterning and transferring technique. The final strain sensor structure is composed of a carbon nanotube nanonet layer between metal electrodes, and vias made on a flexible polyimide substrate (Fig. 3.1). The CNT nanonet acts as the piezoresitive sensing layer and the vias are formed for substrate flexibility enhancement and fabrication ease. In this section, we present the characteristics of the sensor and the experimental results of the new fabrication process.

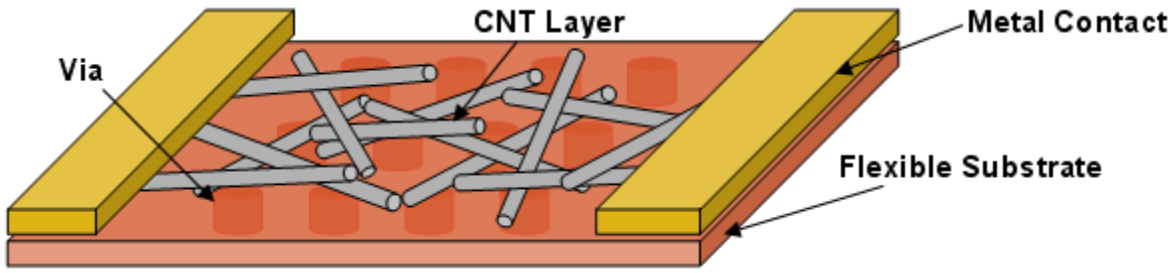

Figure 3.1 Schematic of the CNT strain sensor.

3.1 Characteristics of Proposed Device Design Based on Sensor Criteria

This section describes the characteristics of the proposed device for each critical sensor criterion. These characteristics of interest have been considered to gain insight into how the device will be fabricated, its possible applications, device testing scheme, and also the design of the sensor itself.

3.1.1 Sensitivity and directionality

The embedment of the CNT onto the target material is an important device attribute. Most strain sensors cannot be embedded in the target of measurement: They will be located a finite distance away from the actual surface. Slipping – where the elongation of the target material is greater than that of the strain sensor – is another difficulty for mounting strain sensors on flexible substrates. For these reasons, a strain sensor that cannot be embedded properly in the substrate material has difficulty sensing the actual stress that is applied. To overcome this challenge, CNT strain sensors may be deposited directly on top of a flexible substrate. Because we design the CNT strain sensor in this fashion, we expect this sensor to have high sensitivity.

Crystal-based piezoresistive devices are most sensitive along certain crystalline directions and therefore have limited applications for strain sensors. Any strain that the target experiences off-axis with the crystalline direction will not be sensed. This requires deployment of two sensors, one for each axis. Even with two devices, aligning them to be perpendicular to each other is not a simple task. This becomes even more challenging when the devices are positioned on a flexible substrate, since strain will deform the substrate and induce misalignment of the axes. Thus, the crystalline piezoresistive device approach is not practical for strain sensors on flexible substrates. In contrast, the CNT strain sensor is capable of multidirectional measurement.

Individual CNTs are randomly distributed and thus have a random directionality (Fig. 3.2). Multiple conduction paths are established, which result in multiple axes of strain sensing from a single device. Metal contacts may be patterned at proper locations and angles, and a multidirectional strain sensor is fabricated.

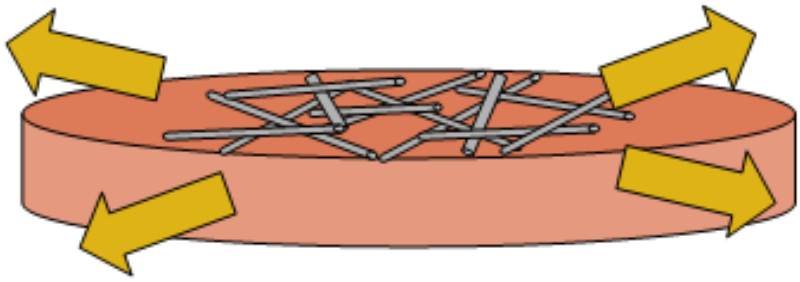

Figure 3.2 Multidirectional strain sensing.

3.1.2 Dynamic range and mechanical flexibility

Conventional metal strain gauges have limited range of operation because excessive elongation results in cracking of the material. Hence, previous strain sensors have been demonstrated for strain levels of less than ~0.5%. With the recent deployment of composites for airplanes and structural materials, SHM applications require larger dynamic ranges.

CNTs are mechanically flexible by nature. Even under severe mechanical deformation, the CNT mesh conducts current. CNT chemical sensors on flexible substrates have been demonstrated with a 2 mm bending radius [20]. The mechanical flexibility increases the dynamic range in which the strain of a material can be measured. Also, the strong embodiment of the CNT on the flexible substrate ensures that before the breaking of the individual CNT, it is more likely for the relative position of adjacent CNTs within the nanonet to be altered, changing the

macroscopic electric resistance. Thus, as long as there is a high density of CNTs within the nanonet, there will be an operational conductive path between the readout metal contacts.

3.1.3 Reliability and linearity

Carbon nanotubes tend to degrade in the presence of oxygen, so a passivation layer is required to properly protect the CNT. In the device design, this limitation must be taken in consideration. As for linearity, previous experiments have demonstrated a linear relationship between voltage output readings and applied strain on CNT buckypaper [31] (Fig. 3.3). This linear relationship simplifies the implementation of the strain sensor and eases device characterization.

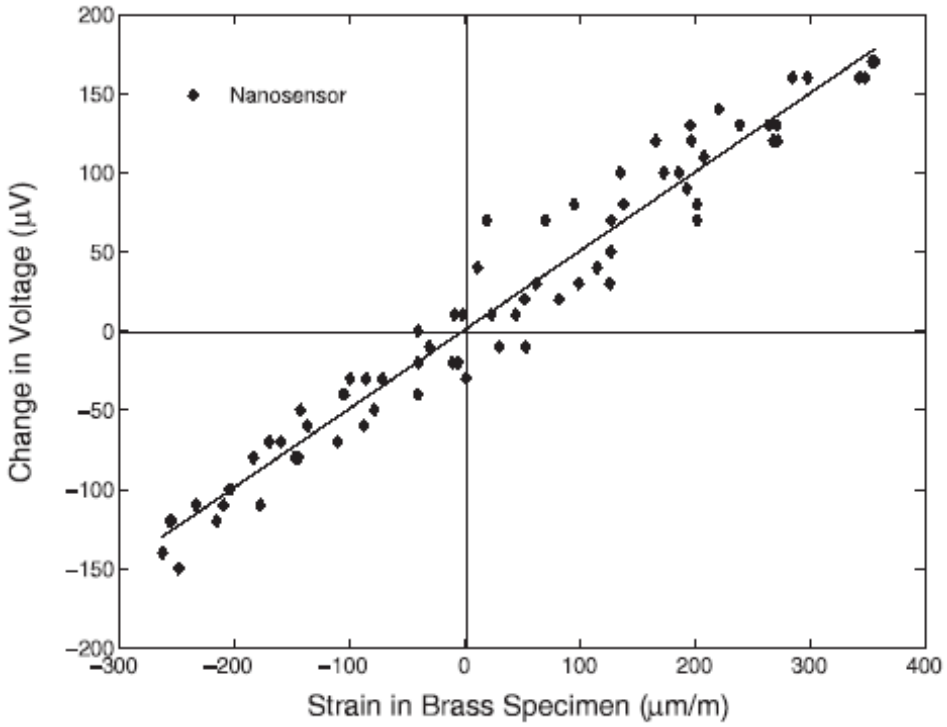

Figure 3.3 CNT strain sensor data [31].

3.2 Fabrication Process for the CNT Strain Sensor

The objective of this project is to fabricate a high performance carbon nanotube based piezoresistive strain sensor on a flexible substrate utilizing novel processing techniques. High mechanical flexibility and strain sensitivity are required. This device also must be practical in terms of fabrication cost. Thus, for practical adaptation to SHM systems, feasibility of large area fabrication must be considered. Fewer fabrication steps, along with clean patterning capability, would also be desirable, giving motive for the use of excimer laser photoablation.

The fabrication of the device starts with CNT deposition by spin-on of CNT solution on the sacrificial substrate. The sacrificial substrate is a Si wafer with 300 nm thick SiO_2 grown by plasma enhanced CVD (PECVD). Afterwards, spin-on polyimide is applied on top. A flexible polyimide substrate is attached, followed by a soft bake process. The CNT-polymer assembly is then patterned by excimer laser photoablation. With high temperature bake, the polyimide now becomes chemically resistant against buffered oxide etch (BOE), prior to the sacrificial release. After BOE etch, metal contacts are formed for the transferred CNT nanonet on flexible polyimide. This section will illustrate the complete fabrication process for CNT strain sensor step by step.

3.2.1 CNT deposition

Carbon nanotubes are deposited on a CVD-grown SiO_2 layer (Fig. 3.4). There are two methods of deposition – liquid-based spin-on CNT and direct CVD growth. The first method is initially used for ease of experimentation. Purified high functionality CNT powder (SWNT, product P3 from Carbon Solutions, Inc., 80-90% purity) is dissolved in DMF solution (1 mg per 1 ml ratio) and then subjected to ultrasound for 3 hours. After the solution is ready, the donor

substrate with SiO_2 layer is cleaned, with standard chemical cleaning of acetone and isopropyl alcohol (IPA) rinse. The solvent is driven out of the substrate with a 3 minute bake on a 125 ^oC hot plate. The sample is then subjected to oxygen plasma ash for thorough removal of organic residue. The CNT solution is applied on the cleaned substrate by using a spin-on process, similar to spinning photoresist for lithography. Multiple spins are done until the desired density is reached. The final sample is then placed on a hot plate for removal of solvents.

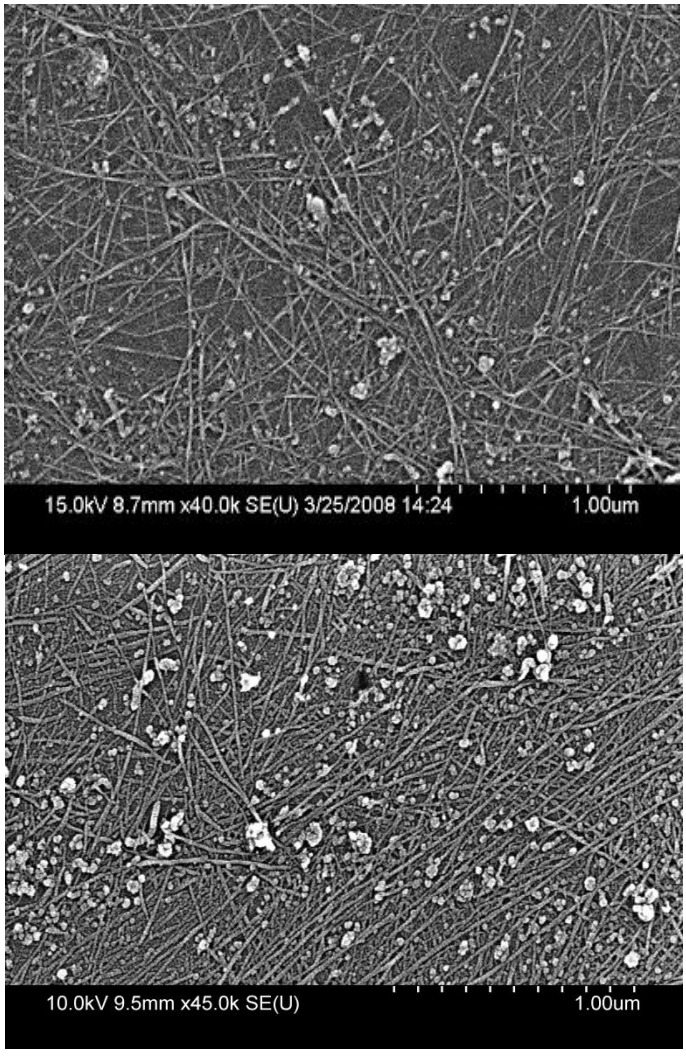

Figure 3.4 Deposition of CNT on SiO_2 sacrificial substrate.

The CNT powder may be dissolved in either water or DMF (Fig. 3.5). While the use of DMF requires chemical hoods for sample preparation, it has several advantages over water. Water produces a solution ratio of 0.1 mg CNT per 1 ml, while DMF produces a solution with a CNT concentration that is 10 times higher. Also, the CNT powder is dispersed homogeneously within DMF; whereas in the case of water solution based spin-on samples, there are aggregated chunks of CNT in certain parts over the wafer. The CNT strain sensor may gain higher sensitivity with a larger CNT nanonet film density, which means that the higher density possible with DMF would be favorable.

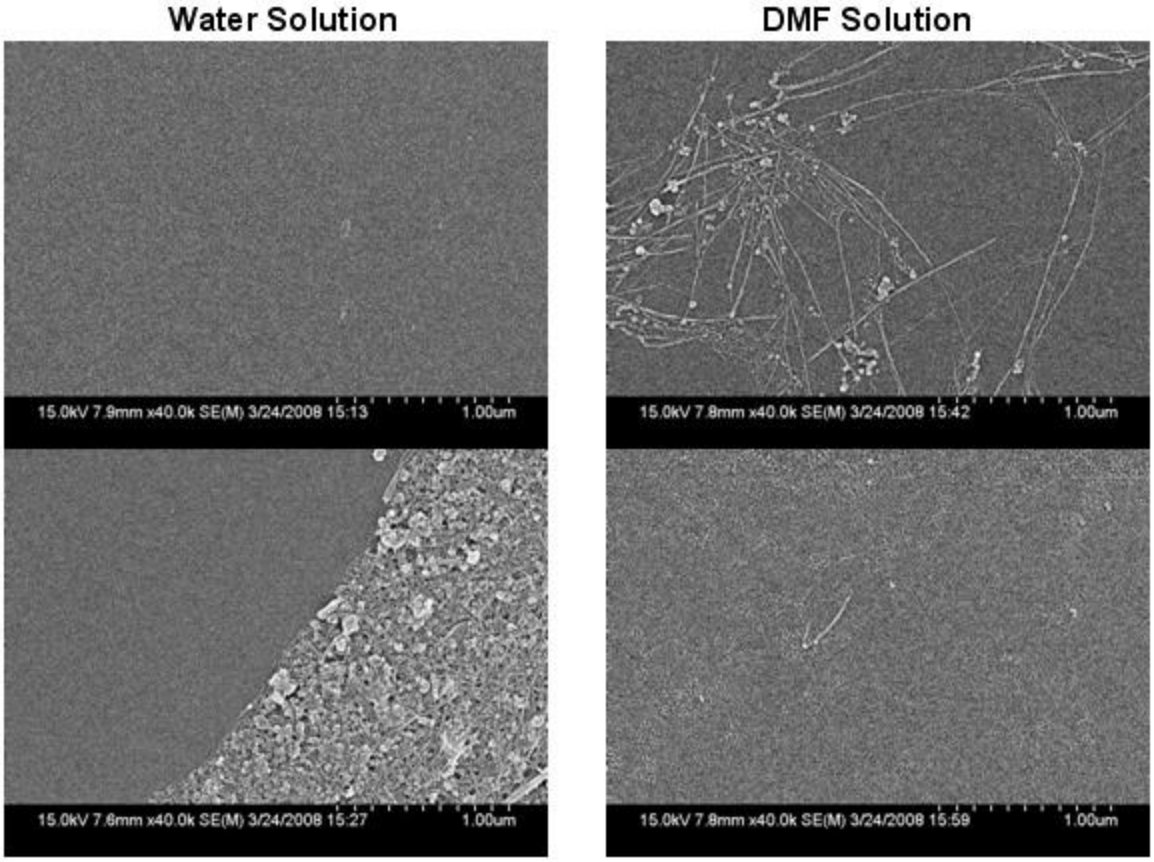

Figure 3.5 Comparison of CNT spin-on by water solution and DMF solution.

To find the best processing conditions, the spin rate (1000, 1500, 2000 rpm), spin time (30, 45, 60 seconds), and dispensing method (drop prior to spinning, dispense while spinning) have been investigated. The resulting film is examined under SEM. Spin speed of 1000 rpm is too slow because droplets of the solution remain on the substrate after the spin (Fig. 3.6). On the other hand, 1500 rpm and 2000 rpm samples did not show this problem. The spin time does not much affect the film quality as long as it is longer than 30 seconds. As for the dropping method, dispensing during spinning gives higher density in select regions, but does not guarantee high density throughout the whole sample. Applying the solution during spin results in nonuniformity of the CNT nanonet film. It is more beneficial to place the solution on the substrate prior to spinning and perform multiple spins for higher density.

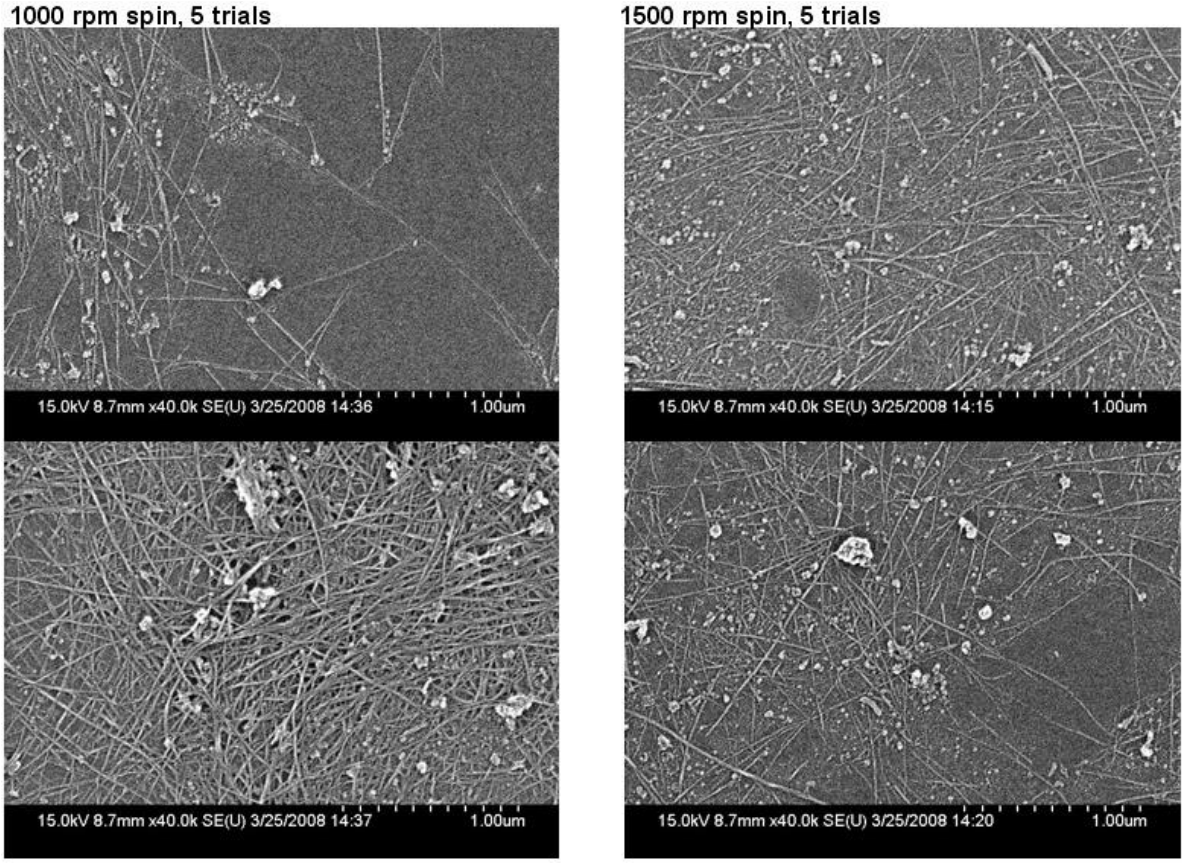

Figure 3.6 Comparison of CNT spin-on by rpm. Note that 1000 rpm results in more nonuniform densities, where some parts are sparse while others are dense.

3.2.2 Adhesion of donor and flexible substrate

A polyimide adhesion layer is spun on the CNT deposited substrate. The spin-on polyimide, PI-2545 (HD Microsystem^{TM}) is spun at 3000 rpm for 30 seconds. The spin-on polyimide serves as an adhesion layer between the CNT and the flexible polyimide substrate (25 µm thickness). The polyimide flexible substrate is gently placed on top of the polyimide-spun CNT-deposited donor substrate. To ensure good adhesion, PI-2545 is softbaked on a hot plate. Note that this step is a soft bake for sacrificial layer and flexible substrate adhesion. An additional high temperature hard bake step is required for chemical resistance. The reason for differentiating the two steps is that whitening may occur during the high temperature polyimide hardbake (Fig. 3.7), which will be discussed in the following sections.

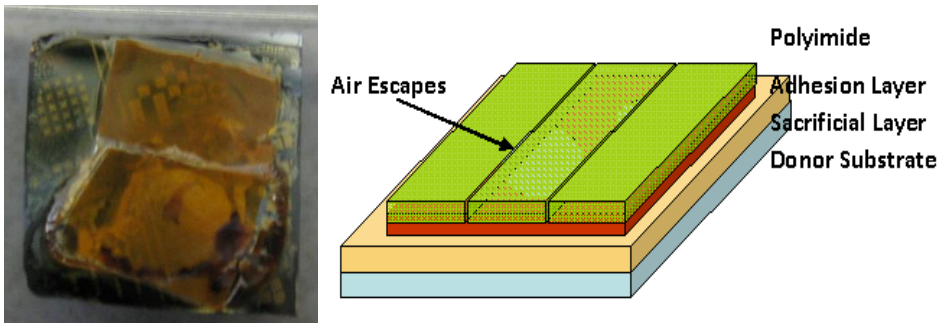

Figure 3.7 Whitening of polyimide in high temperature bake (left); vias for air escape (right).

3.2.3 CNT-polymer substrate patterning by photoablation

The purpose of this step is to pattern the vias and CNT simultaneously with excimer laser photoablation. Vias are formed in the flexible substrate for two reasons: to increase conformability as a mechanical stress release layer, and for fabrication ease. These vias serve as mechanical relief, reducing the stress due to bending of the flexible substrate itself. The stress

reduction allows the device substrate to be elongated further, increasing the device's operation range.

In terms of fabrication advantages, the vias function as an air release layer during high temperature polyimide adhesion hardbake. Without an effective air release layer, the evaporated solvent gas from the spin-on polyimide is trapped between the sacrificial substrate and the flexible substrate. This results in whitening and cracking of the adhesion polymer. Another advantage of the vias is that they provide a path for effective sacrificial layer removal. During the wet etch process, the vias allow the wet etch chemical to reach the sacrificial layer throughout the wafer. Clean patterning of CNTs is also possible with this approach (Fig. 3.8). The CNTs are patterned by the Material Assisted Laser Ablation (MALA) method demonstrated by our research group previously [33]. Previous results produced CNT-polymer composite debris as byproducts of the process. This composite is difficult to remove only with photoresist striping by acetone. In this setup we do not have the limitations of the CNT composite debris. The debris from the CNT ablation step does not cover other device features, since the device features are encapsulated between the flexible polyimide substrate and the sacrificial layer. Also, the debris is easily removed during the sacrificial etch step.

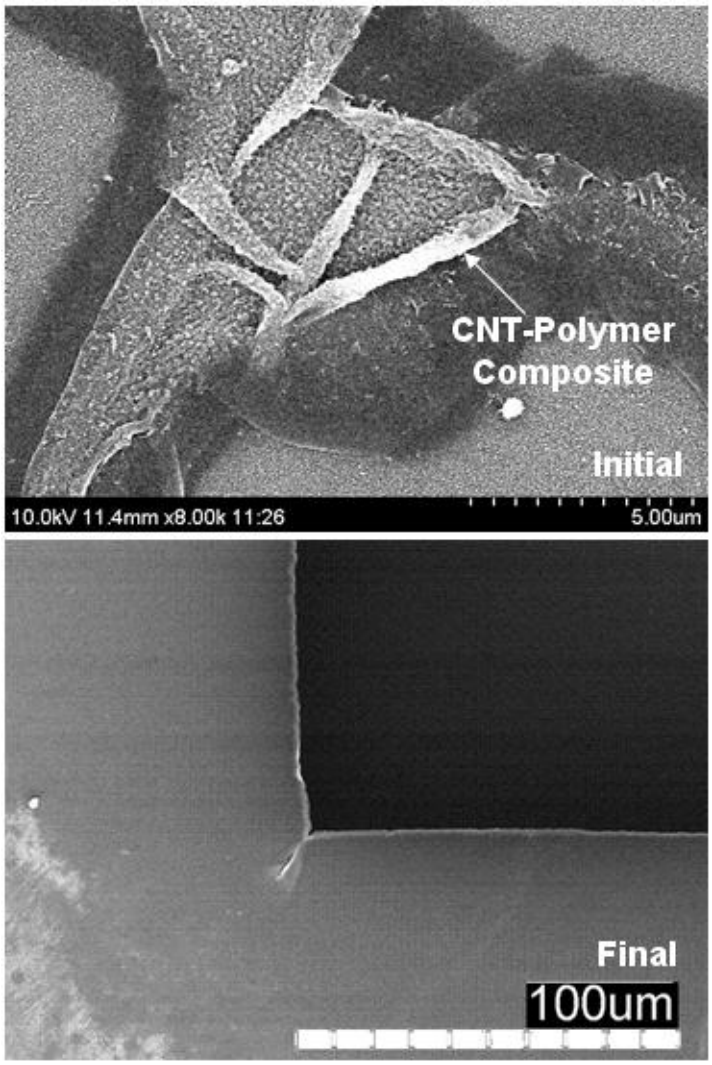

Figure 3.8 CNT-polymer patterning, initial (top) and final (bottom) results.

3.2.4 Adhesion layer hardbake and release of sacrificial layer

After via formation, the sample is placed in oxygen plasma to clean the debris from photoablation. Note that the debris in this case is different from that in the CNT-polymer composites reported in previous experiments. Here, the debris is formed during polymer ablation. The sample is then put on the hotplate for hardbake, at temperatures from 120 ^{o}C up to 370 ^{o}C with a ramp rate of 4 ^{o}C/min. It is held at 370 ^{o}C for 1 hour, and then ramped down to 120 ^{o}C

using the same ramp rate. This process makes the adhesion polyimide chemically inert against the sacrificial layer release step.

The sacrificial layer oxide is etched by 10:1 BOE. The time required for release depends on the sacrificial layer thickness. For 300 nm thick SiO_2, approximately 1 hour is required to finish this process step. After device release, the flexible device is retrieved, washed with DI water, and dried. A final step for dehydration is done, at 120 ^{o}C for 2 minutes. After release, we may examine how well the CNT is transferred to the polyimide layer (Fig. 3.9). The results show that the CNT is transferred with the adhesion layer polyimide in an embedded fashion.

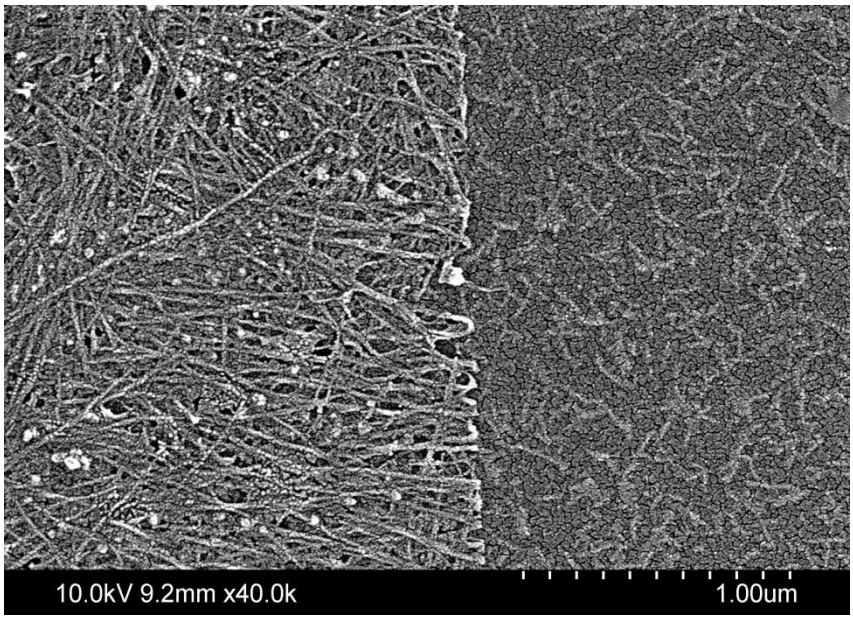

Figure 3.9 Polyimide substrate after CNT transfer. CNT on left, with void on right.

3.2.5 Metal contacts

To fabricate metal contacts, the sample is first patterned with conventional photoresist, with the contact pad region exposed and other portions of the sample covered. An e-beam

evaporator is used to deposit metal contact pads of 100 nm thick gold, with 20 nm Ti to increase adhesion. The formation of TiC also provides lower contact resistance. The metal deposited sample is submerged in acetone to remove the metal in regions other than the contact pad using lift-off.

3.3 Advantages of the New Fabrication Process

In terms of the fabrication process, the technique developed in this project provides several advantages. Since the device fabrication process utilizes a transfer technique, there are fewer thermal limitations in using a flexible substrate. If a process is performed directly on a flexible polymer substrate, all process steps must be below the glass transition temperature of that polymer. Typical polyimide flexible substrates have a maximum processing temperature of 400 ^{o}C. Since the direct growth of CNT is done at ~1000 ^{o}C, it is not possible to process these CNTs on polymer substrates. With the transferring technique, use of high quality CNT is possible.

Efficient transferring is another advantage of the proposed fabrication process. The flexible substrate acts as a stamp itself, thus eliminating one physical transferring step compared to conventional stamping methods. Also, vias provide effective paths for etchant chemicals to reach the sacrificial layer. This enables faster and more uniform release of the sacrificial layer. These vias have additional purposes, such as providing mechanical stress relief of the flexible substrate. This project not only utilizes a novel patterning technique for CNT, Material Assisted Laser Ablation (MALA) [33], but also provides a method to overcome its challenges with CNT-polymer debris residue.

CHAPTER 4

CHARACTERIZATION OF CARBON NANOTUBE STRAIN SENSORS ON FLEXIBLE SUBSTRATES

A CNT strain sensor with high mechanical flexibility has been fabricated (Fig. 4.1). Test setup for strain sensing is prepared, with a platform that supports movement in increments down to 10 µm. The resistances between the two contact pads are measured at various strains. Measurements are taken using this setup to confirm the device characteristic of the new CNT strain sensor.

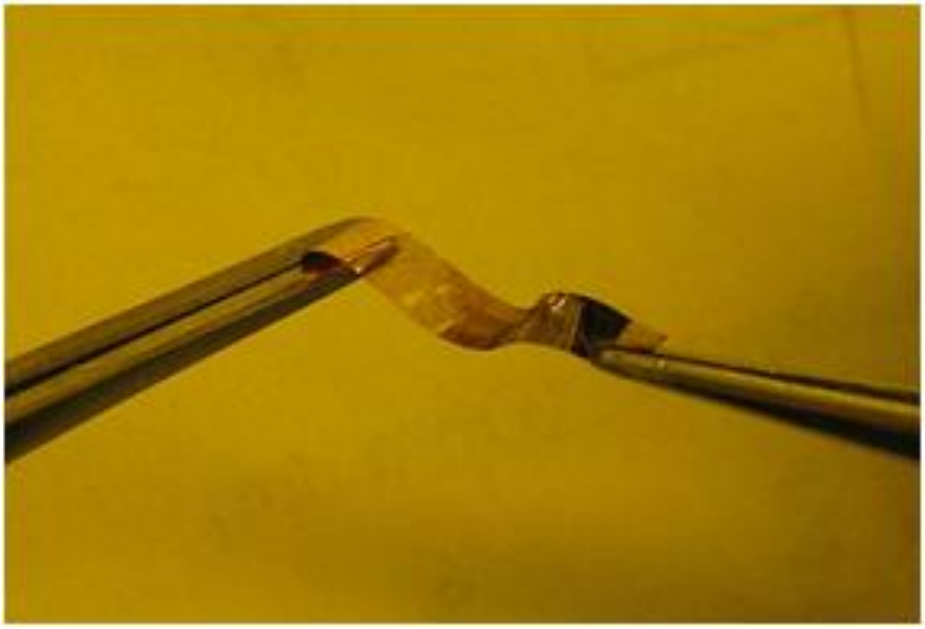

Figure 4.1 Demonstration of the mechanical flexibility of the CNT strain sensor.

4.1 Contact Resistance Between Metal Contact and CNT Nanonet

The measured resistance of the CNT strain sensor consists of two parts: the contact resistance and the CNT nanonet resistance. Only the CNT layer resistance is length-dependent. Multiple contact pads with different distances in between have been fabricated (Fig. 4.2). From this, a data graph of the resistance between the Ti/Au metal contact and the CNT layer as a function of length may be obtained (Fig. 4.3). The contact resistance can be extrapolated as the expected intersection of the data line and the y axis, representing resistance. With a probe station, a constant voltage was applied, and the current was measured. The resistance was calculated using Ohm's law.

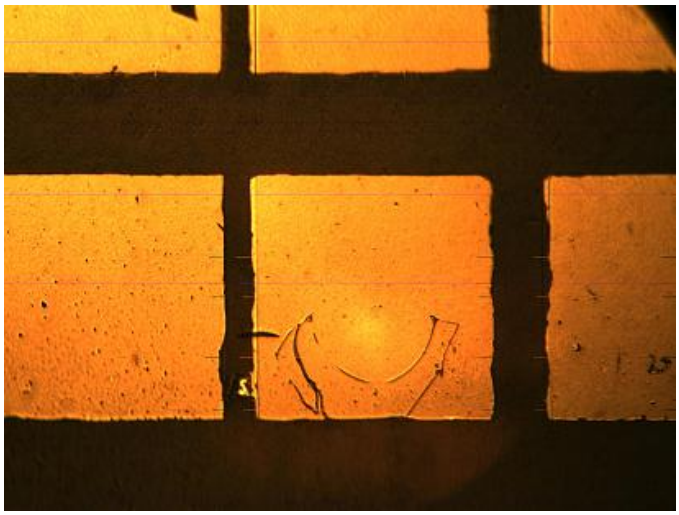

Figure 4.2 Multiple contact pads with different distances in between.

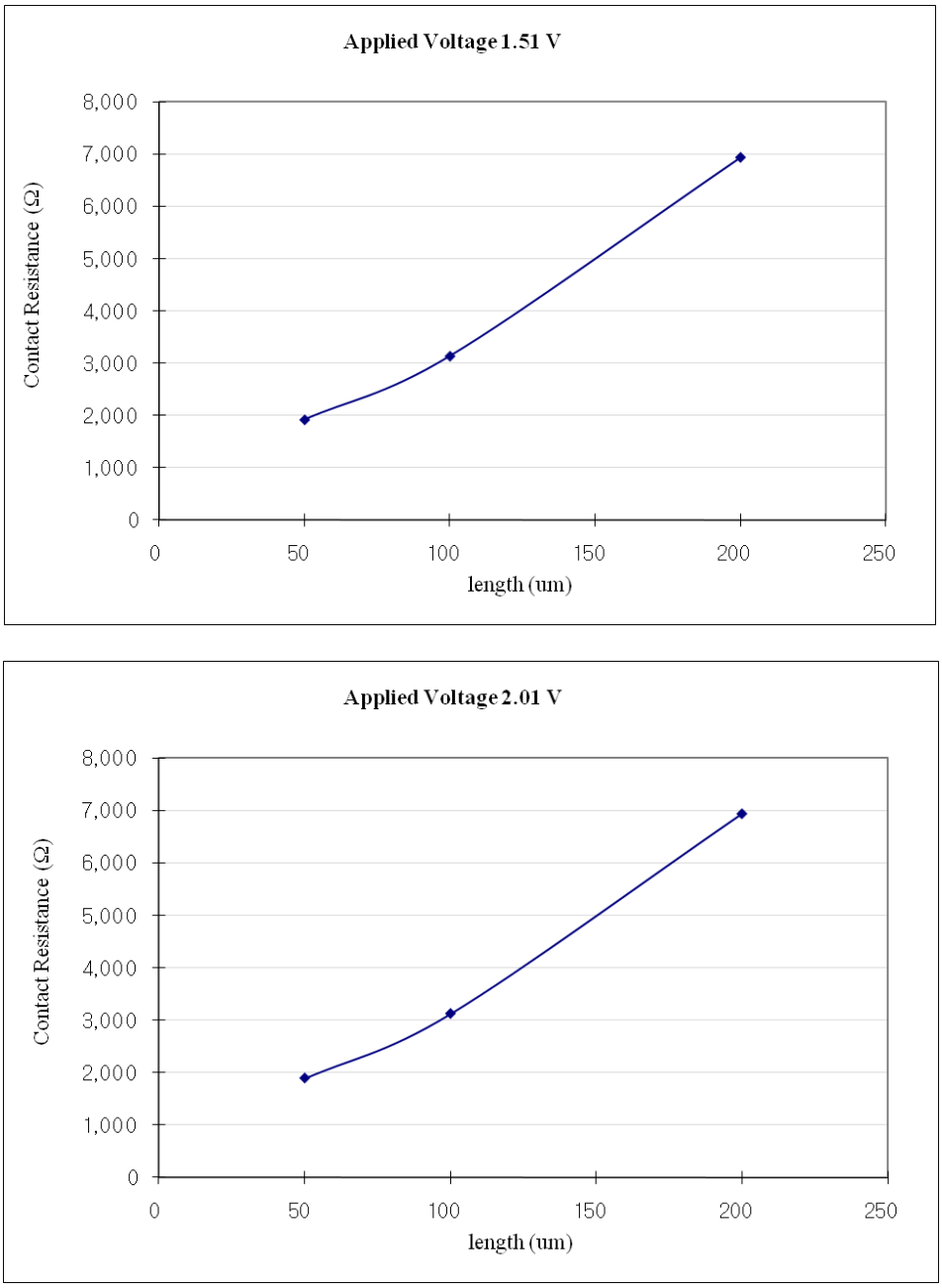

Figure 4.3 Contact resistance data.

The results in Fig 4.3 suggest that the contact resistance is in the vicinity of 1.1 kΩ. The contact pad itself is a 500 µm by 500 µm square. Thus, the contact resistance between the CNT layer and Ti/Cu contact is estimated as 1.38 $\Omega \cdot cm^2$.

4.2 Piezoresistive CNT Strain Sensor Results

The fabricated strain sensor has a high mechanical flexibility, due to the flexible nature of CNTs. With the testing platform (Fig. 4.4, top), the strain and resistance change are recorded. To account for sample slipping out from the testing apparatus, the pixels in the digital camera image are counted for correct strain measurement.

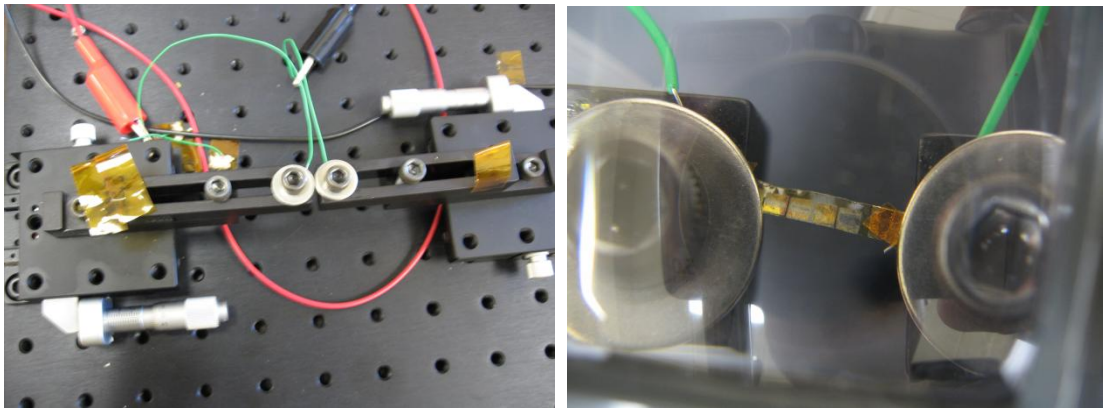

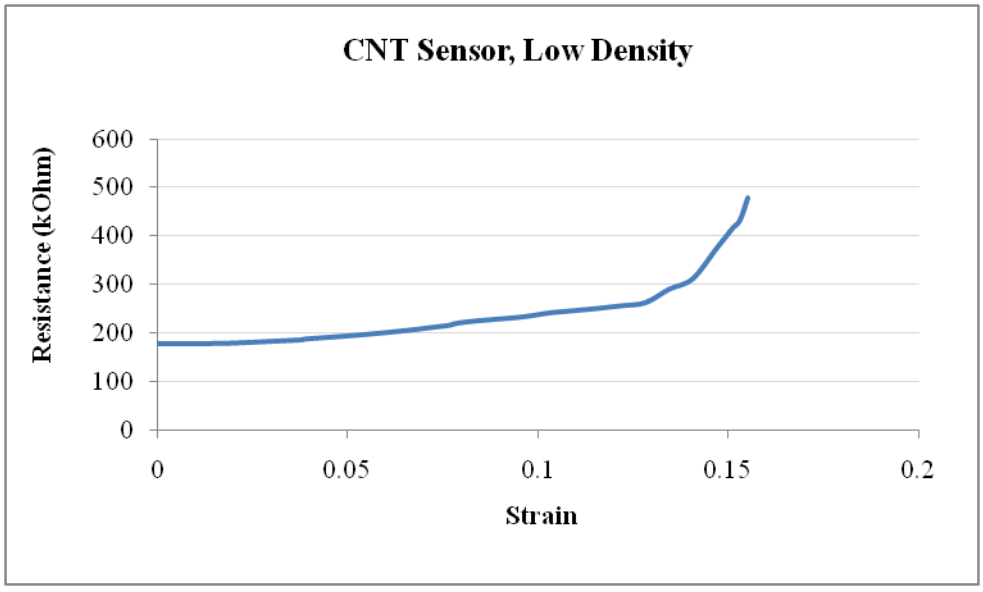

Figure 4.4 Strain testing setup (top); strain sensor results (bottom).

The data in Fig 4.4 can be reorganized to determine the relative resistance, defined as the strain sensor resistance divided by the resistance at zero strain (Fig. 4.5). Also, note that the resistance suddenly changes at higher strain. The reason for the nonlinear behavior is that, because we are testing a flexible substrate based strain sensor, at low strain levels the device is not flat. Only by applying some strain is the device made flat, and the strain sensing occurs afterwards. Hence, the region of interest for the strain sensor is at strain higher than 0.14.

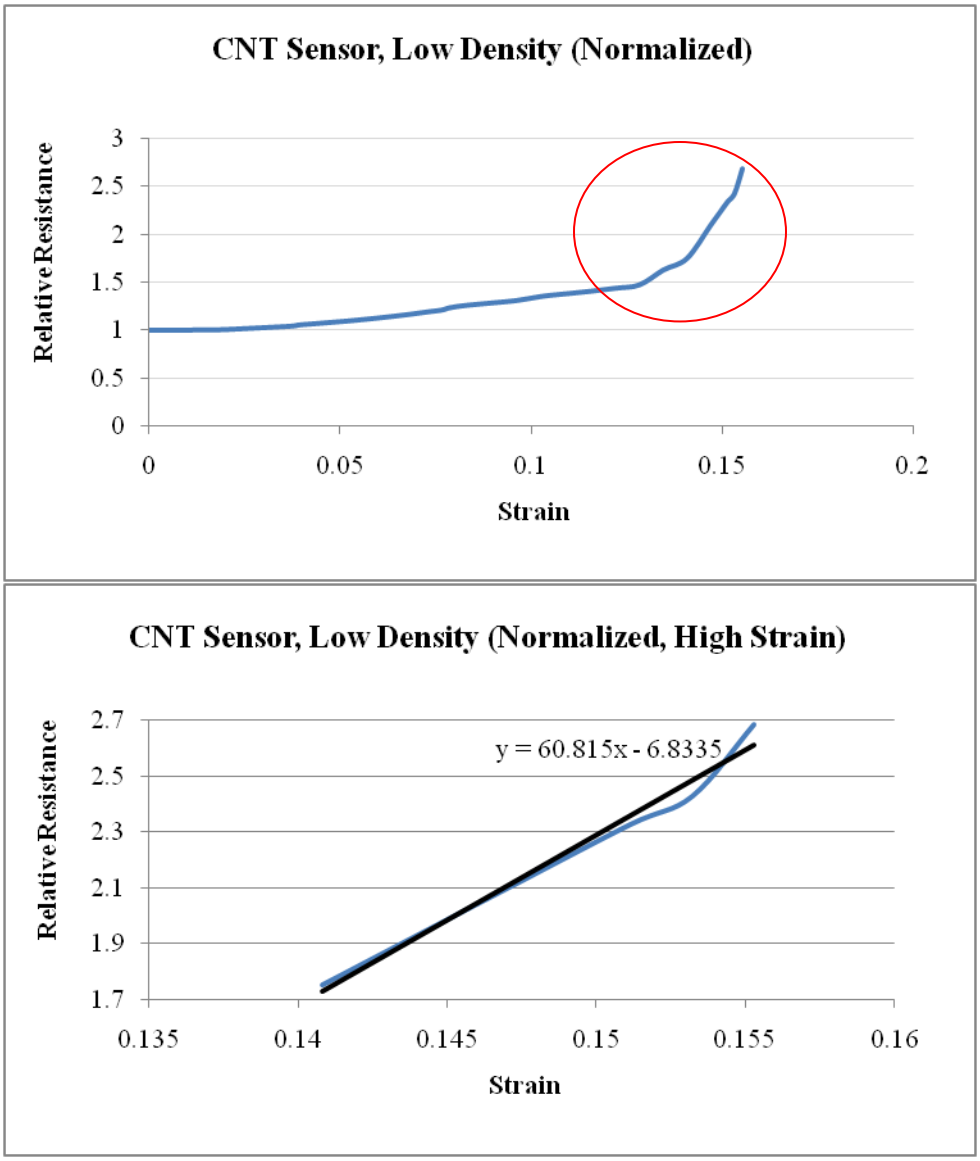

Figure 4.5 Normalized strain sensor data (top); results for straining region (bottom).

From the results in the bottom graph of Fig. 4.5, the slope indicates that the strain gauge factor is 60, with the active strain region from 0.14 to 0.155. This results in a dynamic range of 0.015, or 1.5%, strain. A conventional Si strain gauge has a gauge factor from 50 to 175, and a dynamic range of up to 0.03%. Thus, compared to conventional Si strain gauges, the sensitivity level is similar, but the dynamic range is 50 times wider. Another noteworthy point is that the new CNT strain sensor supports multidirectional sensing, which is not possible with a single Si strain gauge.

CHAPTER 5

CONCLUSIONS

The new CNT strain sensor has several advantages over conventional strain sensors, including multidirectional sensing capability, embedded sensing, greater dynamic range, and increased mechanical flexibility. The new device also has many advantages over previous CNT strain sensors: higher sensitivity, fewer thermal limitations enabling high temperature processes, novel patterning technique of CNT, and efficient transferring processes.

The new fabrication process poses several challenges. The MALA process produces debris during the ablation process. Further experiments using different polymer materials for the MALA process will be done to improve the process. Furthermore, we will research different types of sacrificial layer materials and etchants to increase material compatibility and promote easier heterogeneous integration.

Despite these challenges, the initial results show that the new fabrication methods are effective for the fabrication of an effective CNT strain sensor. The CNT strain sensor has high sensitivity, multidirectional sensing capability, large dynamic range, and is capable of being embedded in many materials. The utilization of the multipurpose vias on a flexible substrate for transferring provides various advantages including mechanical stress relief and ease of fabrication. We will continue the fabrication experiments with different materials and designs, to optimize the processes that yield the best device results. We will investigate CNTs for additional

sensor nodes, such as chemical and biological sensors. We will also experiment with various driving circuitry configurations to determine the optimal method for sensor readout. After testing these discrete sensors, we will construct a working prototype and perform application-specific tests on it.

As a final goal, we envision a "smart skin" sensor array system with several different sensor nodes, robust interconnect strategies, data acquisition and communication circuitry, and power harvesting circuitry for a versatile and reliable system that can be implemented into a wide range of applications. This sensor array will be flexible and stretchable to conform to a variety of surfaces, and it will be robust, so that damage to one area of the sensor will not affect the operation of the entire system. Furthermore, the sensor array will be able to communicate effectively with other sensor arrays and reliably deliver data wirelessly to a data acquisition system. We also foresee this approach to be cost-effective such that the sensor system will be practical and commercially available for the applications we have discussed.

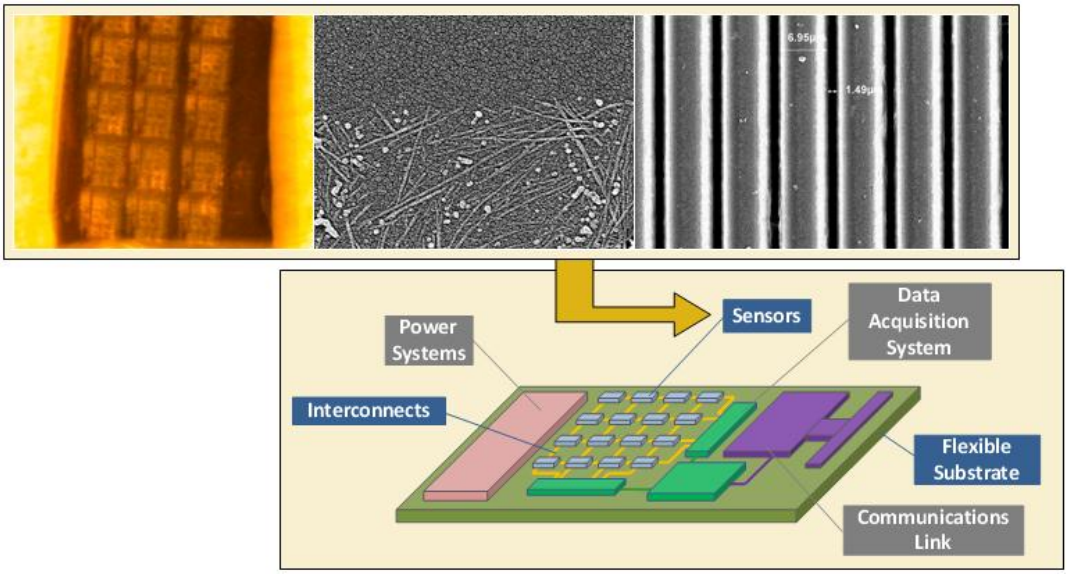

Figure 5.1 Concept of the smart skin project.

REFERENCES

[1] K. Huang and P. Peumans, "Stretchable silicon sensor networks for structural health monitoring," in *Smart Structures and Materials 2006: Sensors and Smart Structures Technologies for Civil, Mechanical, and Aerospace Systems*, 1997, p. 617412.

[2] A. Kumar et al., "Potential applications of smart layer technology for homeland security," in *Nondestructive Detection and Measurement for Homeland Security II*, 2004, pp. 61-69.

[3] V. Giurgiutiu, J. M. Redmond, D. P. Roach, and K. Rackow, "Active sensors for health monitoring of aging aerospace structures," in *Smart Structures and Materials 2000: Smart Structures and Integrated Systems*, 2000, pp. 294-305.

[4] R. Thirumalainambi et al., "Non-intrusive techniques of inspections during the pre-launch phase of space vehicle," in *Modeling, Simulation, and Verification of Spacebased Systems II*, 2005, pp. 92-99.

[5] S. Winkler et al., "Multiple sensor fusion for autonomous mini and micro aerial vehicle navigation," in *TE4CO4 2005-2005 IEEE Region 10 Conference*, 2005, p. 4084899.

[6] R. Michelson and S. Reece, "Update on flapping wing micro air research-ongoing work to develop a flapping wing crawling 'Entomopter'," in *Proceedings of RPV/UAV Systems (C) Remotely Piloted Vehicles/Unmanned Airborne Vehicles*, 1998, pp. 301-311.

[7] J. Dhainaut et al., "Measuring aeroelastic wing characteristics using Microsensor Systems (MEMS)," in *45th AIAA Aerospace Sciences Meeting 2007*, Reno, NV, 2007, pp. 15119-15133.

[8] T. Hoshi and S. Hiroyuki, "Robot skin based on touch-area-sensitive tactile element," in *2006 IEEE International Conference on Robotics and Automation*, 2006, pp. 3463-3468.

[9] H.-K. Lee et al., "A flexible polymer tactile sensor: Fabrication and modular expandability for large area deployment," *Journal of Microelectromechanical Systems*, vol. 15, pp. 1681-1686, Dec. 2006.

[10] S. Lobodzinski and M. Kuzminska, "Silicon whole body sensors for medical applications – A glimpse of the future," in *Proceedings of the 1998 WESCO4 Conference*, 1998, pp. 286-291.

[11] H. Zhang et al., "Design of a flexible stethoscope sensor skin based on MEMS technology," in *2006 7th International Conference on Electronics Packaging Technology, ICEPT '06*, 2006, p. 4198956.

[12] M. V. Scanlon, "Acoustic sensor pad for physiological monitoring," in *Proceedings of the 1997 19th Annual International Conference of the IEEE Engineering in Medicine and Biology Society*, 1997, pp. 747-750.

[13] M. Meng et al., "Intelligent textiles based on MEMS technology," in *57th Electronic Components and Technology Conference 2007, ECTC '07*, 2007, pp. 2030-2034.

[14] G. Olafsdottir et al., "Multisensor for fish quality determination," *Trends in Food Science and Technology*, vol. 15, pp. 86-93, Feb. 2004.

[15] C. Sheridan et al., "Detection of premature browning in ground beef using an optical-fibre based sensor," in *EWOFS 2007: Third European Workshop on Optical Fibre Sensors*, 2007, p. 66193R.

[16] M. Suman et al., "MOS-based artificial olfactory system for the assessment of egg products freshness," *Sensors and Actuators, B Chemical*, vol. 125, pp. 40-47, July 16, 2007.

[17] C. Liu, *Foundations of MEMS.* Upper Saddle River, NJ: Pearson Education, Inc., 2006.

[18] J. H. Ahn et al., "Heterogeneous three-dimensional electronics by use of printed semiconductor nanomaterials," *Science*, vol. 314, p. 1754, 2006.

[19] Y. Chai et al., "Flexible transfer of aligned carbon nanotube films for integration at lower temperature," *Nanotechnology*, vol. 18, p. 355709, 2007.

[20] Q. Cao et al., "Medium-scale carbon nanotube thin-film integrated circuits on flexible plastic substrates," *Nature*, vol. 454, pp. 495-500, July 24, 2008.

[21] J. Engel et al., "Polymer-based MEMS multi-modal sensory array," *Polymer Preprints*, vol. 44, no. 2, pp. 534-535, 2003.

[22] Y. Kanda, "Piezoresistance effect of silicon," *Sensors and Actuators A: Physical*, vol. 28, pp. 83-91, 1991.

[23] L. Zou et al., "Structural health monitoring of pipeline with distributed Brillouin sensor," in *Structural Health Monitoring and Intelligent Infrastructures*, Z. Wu and M. Abe, Eds. Lisse, The Netherlands: Swets and Zeitlinger B. V., 2003, pp. 65–71.

[24] A. Mufti, "Integration of sensing in civil structures: Development of the new discipline of Civionics," in *Structural Health Monitoring and Intelligent Infrastructures*, Z. Wu and M. Abe, Eds. Lisse, The Netherlands: Swets and Zeitlinger B. V., 2003, pp. 65-71.

[25] M. J. Schulz et al., *Nanoengineering of Structural, Functional and Smart Materials*. Boca Raton, FL: CRC Press, 2005.

[26] M. S. Dresselhaus, *Carbon Nanotubes: Synthesis, Structure, Properties, and Applications*. New York, NY: Springer-Verlag, 2001.

[27] V. Gayathri and R. Geetha, "Carbon nanotube as NEMS sensor – effect of chirality and stone-wales defect intend," *Journal of Physics: Conference Series*, vol. 34, pp. 824-828, 2006.

[28] Y. Nakayama, "Plasticity of carbon nanotubes: Aiming at their use in nanosized devices," *Jap. Jour. of Appl. Phys*., vol. 46, no. 8A, pp. 5005-5014, 2007.

[29] I. Kang, "Building smart materials using carbon nanotubes," *Smart Electronics, MEMS, and BioMEMS, and Nanotechnology Conference*, 2004, vol. 5389, pp. 167-175.

[30] K. Liao and S. Li, "Interfacial characteristics of a carbon nanotube-polystyrene composite system," *Applied Physics Letters*, vol. 79, no. 50, pp. 4225-4227, 2001.

[31] P. Dharap et al., "Nanotube film based on single-wall carbon nanotubes for strain sensing," *Nanotechnology*, vol. 15, pp. 379-382, 2004.

[32] K. L. Lu et al., “Mechanical damage of carbon nanotubes by ultrasound,” *Carbon*, vol. 34, p. 814, 1996.

[33] J. Chae et al., “Patterning of single walled carbon nanotubes using a low-fluence excimer laser photoablation process,” *Applied Physics Letters*, vol. 92, pp. 173115/1-173115/3, 2008.